Proc. Natl. Acad. Sci. USA
Vol. 91, pp. 11308–11312, November 1994
Neurobiology

Activity-dependent current distributions in model neurons

(activity-dependent regulation/neuronal plasticity/calcium-dependent modulation/channel density)

MICAH SIEGEL*, EVE MARDER, AND L. F. ABBOTT†

Center for Complex Systems, Brandeis University, Waltham, MA 02254

Communicated by John J. Hopfield, August 15, 1994

ABSTRACT **The electrical activity of a neuron can affect its intrinsic physiological characteristics through a wide range of processes. We study a computer-simulated multicompartment model neuron in which channel density depends on local Ca^{2+} concentrations. This has three interesting consequences for the spatial distribution of conductances and the physiological behavior of the neuron: (*i*) the model neuron spontaneously develops a realistic, nonuniform distribution of conductances that is linked both to the morphology of the neuron and to the pattern of synaptic input that it receives, (*ii*) the response to synaptic input reveals a form of intrinsic localized plasticity that balances the synaptic contribution from dendritic regions receiving unequal stimulation, and (*iii*) intrinsic plasticity establishes a biophysical gain control that restores the neuron to its optimal firing range after synapses are strengthened by "Hebbian" long-term potentiation.**

The electrical characteristics of a neuron depend on the density and distribution of its ion channels. For a neuron to develop and maintain a specific repertoire of functional characteristics, ion channels must be continually synthesized, transported to appropriate sites, and inserted into the cell membrane. Active channels can be modulated by phosphorylation (1, 2) and removed from duty through membrane internalization (3). It is known that cell–cell interactions can play an important role in controlling the distribution of transmitter receptors and ion channels on nerve and muscle cells (4–6) through a complex series of molecular and cellular mechanisms. Another critical factor that may influence channel densities and distributions is the activity of the neuron (7–11). We have previously developed a Ca^{2+}-dependent regulation scheme (12, 13) to model the effects of activity on membrane conductances. In single-compartment isopotential model neurons, this regulation has a number of interesting properties. Model neurons with activity-dependent conductances can spontaneously develop the conductances needed to perform a specific function, they can respond to external perturbations by adjusting their conductances to maintain a desired level of activity, and, in small neuronal circuits, they can spontaneously differentiate to develop different properties in response to synaptic input (12, 13). Here we explore the consequences of neuronal structure on the spatial distribution of membrane currents, using a multicompartment model neuron.

MODEL

We consider a multicompartment model neuron (14) with the morphology of a hippocampal CA1 pyramidal cell. The model neuron has fast Na^+ (I_{Na}), delayed-rectifier K^+ (I_K), transient K^+ (I_A, for Fig. 3 only), voltage-dependent Ca^{2+} (I_{Ca}), and leakage currents (I_L). To model the effects of activity-dependent processes affecting channel distribution, we assume that the maximal conductances of I_{Na}, I_K, and I_A are dynamic variables regulated by the local intracellular Ca^{2+} concentration (12, 13). We use Ca^{2+} as the feedback element linking activity to conductances because the average intracellular Ca^{2+} concentration is highly correlated with the electrical activity of the neuron (12, 15) and because Ca^{2+} is ubiquitous in biochemical pathway regulation and plays a role in many processes relevant to channel regulation (1, 2, 7–11). Although in our model Ca^{2+} alone regulates the feedback, in biological neurons several second messengers may act in concert to play this role.

The maximal conductances in the model approach steady-state values that are increasing sigmoidal functions of calcium concentration for I_K and I_A and decreasing sigmoidal functions for I_{Na}. The time constant controlling the approach to the steady state is much larger than any other time scale characterizing the behavior of the neuron. As a result, significant activity-induced shifts of conductances occur only when the neuron experiences prolonged periods of modified activity.

I_{Na}, I_K, and I_A are expressed in the standard form (16)

$$I = \bar{g} \cdot m^p \cdot h^q \cdot (V - E_r),$$

with $E_r = 50$ mV for the Na^+ current and $E_r = -70$ mV for the K^+ currents. The maximal conductances $\bar{g}$, rather than constant parameters as in most neuron models, are here dynamic variables that obey the differential equations (12, 13)

$$\tau \frac{d\bar{g}}{dt} = \frac{G}{1 + \exp[\pm([Ca^{2+}] - C_T)/\Delta]} - \bar{g},$$

where the variable sign is plus with $G = 360$ mS/cm^2 for I_{Na} and minus with $G = 180$ mS/cm^2 for I_K. The time constant τ controls the rate of activity-dependent modification and is likely to be on the order of many minutes to hours in real neurons. However, to speed up our simulations, we took $\tau =$ 10 s; we have confirmed that this does not affect our results. The parameters $C_T = 0.5$ μM and $\Delta = 0.6$ μM determine the shape and position of the sigmoidal curve for the equilibrium value of $\bar{g}$ as a function of intracellular Ca^{2+} concentration.

The Ca^{2+} current in the model is patterned after that of the Morris–Lecar model (17)

$$I_{Ca} = \bar{g}_{Ca}(1 + \tanh[(V - V_1)/V_2]) \cdot (V - E_{Ca}),$$

where $V_1 = -50$ mV, $V_2 = 10$ mV, and $E_{Ca} = 150$ mV. For the results shown here, the maximal conductance of the Ca^{2+} current was fixed and uniform, $\bar{g}_{Ca} = 0.03$ mS/cm^2. The intracellular Ca^{2+} concentration satisfies a diffusion equation with exponential Ca^{2+} removal and uptake,

The publication costs of this article were defrayed in part by page charge payment. This article must therefore be hereby marked "*advertisement*" in accordance with 18 U.S.C. §1734 solely to indicate this fact.

*Present address: Computation and Neural Systems Program, California Institute of Technology, Pasadena, CA 91125.
†To whom reprint requests should be addressed.

$$\frac{\partial[Ca^{2+}]}{\partial t} = D\frac{\partial^2[Ca^{2+}]}{\partial x^2} - k[Ca] - \gamma I_{Ca},$$

where γ converts from current to Ca^{2+} concentration, $D = 6 \times 10^{-6}$ cm^2/s, and $k = 1/600$ ms (18, 19). We set all of these parameters constant through all compartments in the model and, as we mention in the next section, the results described below are qualitatively insensitive to their values through a wide range.

RESULTS

Self-Organizing Conductance Distributions. Because the maximal conductances in any region of the model neuron depend on the average local intracellular Ca^{2+} concentration, the distribution of membrane conductances is determined by the electrical activity and morphology of the cell. Fig. 1 shows distributions of Na^+ and K^+ conductances that arise spontaneously in the model for two patterns of synaptic stimulation. Initially, we set the maximal Na^+ and K^+ conductances to zero (Fig. 1*A*). During the simulation, we applied random Poisson-distributed synaptic inputs over the apical and basal dendritic trees of the model neuron. As the simulation progressed, the maximal conductances changed in response to the intracellular calcium concentration until a steady state was established. The steady-state conductance distributions (Fig. 1 *B* and *C*) are nonuniform, with I_{Na} concentrated at the soma, I_K concentrated in the dendritic arbor, and relatively uniform conductances along the axon. The soma and initial segment of the axon can initiate action potentials and the axon can conduct action potentials (for a different approach to constructing an axon, see ref. 20). Thus an initially passive and electrically homogeneous model neuron can spontaneously develop active, nonuniform substructures driven solely by effects of morphology and activity and mediated through intracellular Ca^{2+}.

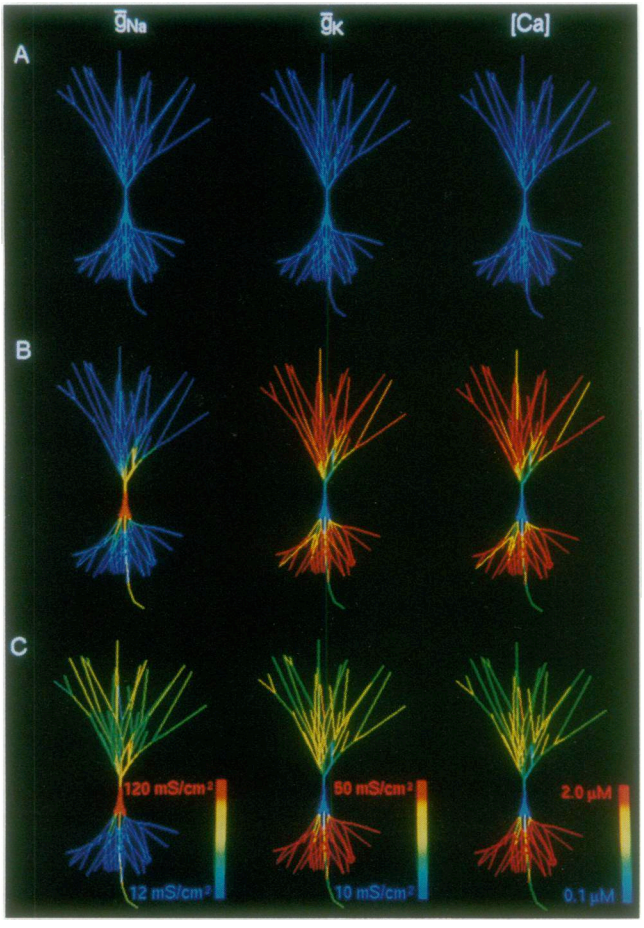

FIG. 1. Distribution of conductances produced by the model. The three columns show the distribution of maximal Na^+ conductances ($\bar{g}_{Na}$), maximal K^+ conductances ($\bar{g}_K$), and the average intracellular Ca^{2+} concentration ([Ca]). (*A*) Initially the model neuron had a uniform Ca^{2+} conductance but no Na^+ or K^+ conductances. (*B*) The steady-state conductance distribution following prolonged 100-Hz stimulation of synapses with 2-nS peak conductance randomly placed on the basal and apical dendrites. (*C*) The steady-state conductance distribution following prolonged stimulation of randomly placed 2-nS synapses at 100 Hz on the basal dendrites and 5 Hz on the apical dendrites. Note that experimentally induced Ca^{2+} transients would be superposed on the average Ca^{2+} distributions given above.

I_{Na} seen in Fig. 1 *B* and *C* is large near the soma because the large somatic volume acts as a Ca^{2+} sink, keeping the concentration there fairly low. I_K is large in the dendrites because the background synaptic stimulation and small diameters keep the average Ca^{2+} concentration high. Depending on the geometry of the neuron and the pattern of synaptic input we give, heterogeneous "hot" and "cold" spots sometimes develop along the dendritic arbor. The axon is more uniform, since this region has a relatively constant average intracellular Ca^{2+} concentration. $\bar{g}_{Na}$ is high in the first 10–20 μm of the axon, to form a spike-initiation region. This length scale is determined by Ca^{2+} removal and diffusion properties. Although our model of Ca^{2+} uptake is too simple to be considered realistic, the final Ca^{2+} concentrations in Fig. 1 are low in the soma and rise in the proximal dendritic region similar to those measured in stimulated hippocampal neurons (21). Experimental results show a drop in the distal dendritic Ca^{2+} concentration (21) not found in our model. The declining Na^+ current density along the proximal dendrites agrees qualitatively with inferred distributions in hippocampal neurons (18, 19, 21).

Effects of Local Activity. A comparison of Fig. 1 *B* and *C* illustrates the effect of activity on the distribution of conductances. The distribution in Fig. 1*B* arose when the apical and basal dendrites were stimulated equally. The resulting current distributions are similar for the two trees. The conductances shown in Fig. 1*C* resulted from a prolonged period during which the apical arbor received synaptic input at a lower frequency than the basal arbor. The lower rate of synaptic stimulation in the apical dendrites caused a lower local intracellular Ca^{2+} concentration and hence a larger Na^+ current and smaller K^+ current in that region.

Fig. 2 demonstrates the functional significance of the activity-dependent distribution of dendritic currents seen in Fig. 1. We applied a test stimulation to both apical and basal dendritic arbors of the neurons shown in Fig. 1 *B* and *C*. This produced similar, passive excitatory postsynaptic potentials (EPSPs) in both dendrites for the conductance distribution of Fig. 1*B* (Fig. 2*A*). By contrast, EPSPs in the apical dendrite of the neuron in Fig. 1*C* are amplified nonlinearly by active processes leading, in this example, to the echo of a delayed somatic action potential (Fig. 2*B*). Local activity-dependent conductances balance contributions coming from dendritic trees, or regions of individual dendrites. Heavily stimulated regions become leaky and require strong synaptic inputs to significantly depolarize the soma. Regions that receive chronically weak stimulation become less leaky—or even active—and are much more effective at transferring synaptic depolarization to the soma.

Gain Control. We find that activity-dependent conductances can also act as gain control elements to set the neuronal response relative to a background synaptic input level. This has important implications when coupled with ideas about the role of synaptic plasticity in learning and memory. In Fig. 3 we randomly divided the input synapses

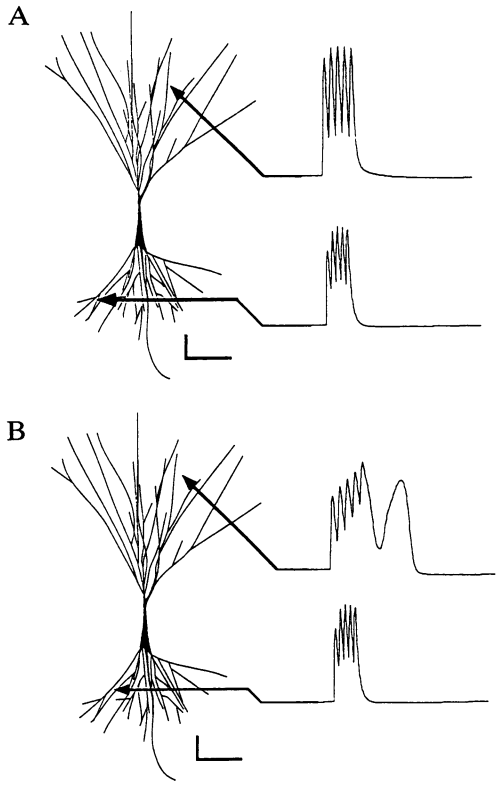

FIG. 2. Test stimulation of the neurons in Fig. 1 *B* and *C*. (*A*) The model neuron with conductances distributed as in Fig. 1*B* received a series of five synaptic stimuli in the apical and basal dendrites. Responses were similar in the two dendritic regions. (*B*) The model neuron with conductance shown in Fig. 1*C* was stimulated as in *A*. In this case, the test stimuli show that the basal dendrite responded passively, whereas the apical dendritic response was nonlinearly amplified and gave rise to a somatic action potential (the electrotonic echo of which can be seen). Scale bars: 5 ms and 5 mV.

into two groups or patterns, p_1 and p_2. Initially, high-frequency stimulation of one group of synapses combined with low-frequency stimulation of the other group fired the neuron, but low-frequency background stimulation of both groups failed to do so (Fig. 3*A*). We then potentiated the p_1 synapses to simulate "Hebbian learning" of this pattern of stimulation. We denote the potentiated synapses by P_1. After potentiation, high-frequency stimulation of the P_1 synapses produced high-frequency firing. However, because of the strength of the potentiated P_1 synapses, low-frequency stimulation of P_1 also fired the cell when accompanied either by high- or low-frequency stimulation of p_2 (Fig. 3*B*). This illustrates a common problem associated with modification of synaptic strengths: potentiated synapses may become strong enough to dominate other synaptic inputs and saturate the response of the neuron. Saturation is a problem endemic to any physical system with limited dynamic range. A neuron with many potentiated synapses may respond to virtually any synaptic input by firing near its maximal rate, thereby losing the ability to code information through a graded firing rate. Conversely, a neuron with strongly depressed synapses may stop firing altogether and drop out of network activity.

Fig. 3*C* illustrates that activity-regulated conductances can ameliorate this problem. We exposed the model neuron to low-frequency, background stimulation of both P_1 and p_2 synapses for a prolonged period. The initially elevated electrical response to these background inputs following potentiation of the P_1 synapses slowly down-regulated the Na^+ conductances and up-regulated the K^+ conductances throughout the cell. After this gain control regulation, neither the background stimulus nor the "unlearned" pattern p_2 produced firing; only the "learned" pattern P_1 fired the neuron (Fig. 3*C*). The activity-dependent currents eliminated the excessive background-induced activity allowing the neuron to respond selectively to the learned input pattern.

Robustness. We have tested these results over a wide range of parameter values and in three different cells, and we find that the physiological behavior and the conductance distribution is stable through diverse extrinsic and intrinsic conditions. The model neuron converges to its steady-state conductance distributions independent of the initial conductance distributions we choose for the model (e.g., Fig. 1 *B* and *C* do not depend on Fig. 1*A*; we took the initial conductance distribution in Fig. 1*A* for simplicity). The final conductance distribution and physiological behavior of the cell are essentially unaffected by variations over orders of magnitude in the various electrical parameters characterizing the passive membrane.

We also ran numerical simulations in which $\bar{g}_{Ca}$, the maximal conductance of I_{Ca}, varies as a Ca^{2+}-dependent dynamic variable like other currents in the model. Because in our model I_{Ca} is a small fraction of the total electrical current carried into the cell, the steady-state conductance distribution is unaffected by this change. We find that the local distribution grows smoother when I_{Ca} becomes the dominant electrical current. With a spatially uniform exponential uptake mechanism for Ca^{2+}, the two parameters governing the diffusion and uptake of Ca^{2+} set the effective length scale over which conductances vary in the model cell; the overall conductance distribution is also qualitatively independent of these parameters. A more complicated buffer distribution or kinetic model of Ca^{2+} buffering and diffusion would affect the distribution of free Ca^{2+} and therefore would change the distribution of conductances in our model cell. Nevertheless, it is interesting that the simplistic first-order model used here produces anything that resembles a verisimilar channel distribution.

DISCUSSION

Our modeling studies indicate that the local Ca^{2+} concentration can regulate conductances effectively to produce three interesting effects. (*i*) Realistic, nonuniform current distributions develop spontaneously on the basis of local intracellular Ca^{2+} concentrations that depend on both electrical activity and cell morphology. This suggests that the time-averaged Ca^{2+} concentration in a region of a neuron may shape the types and strengths of conductances in that area. (*ii*) Different spatial patterns of stimulation produce different distributions of conductances. As a result, the depolarization delivered to the soma from a given dendritic region depends on the strength of a synaptic input relative to the chronic background level in that region rather than solely on the absolute strength of the input. (*iii*) Activity-dependent regulation acts as a gain control mechanism to compensate for the effects of long-term synaptic potentiation and depression. The model discussed here suggests a plausible biophysical mechanism for the neuron to make this gain adjustment automatically. It could be augmented by including slow, Ca^{2+}-dependent regulatory effects on synaptic strengths as well.

We do not mean to imply that neuronal structure and activity in themselves determine the distribution and number of channels in biological neurons and networks. The effects of trophic factors, growth factors, and hormones will modify second-messenger pathways and therefore will be integrated with the direct effects of activity. Thus the molecular environment may sculpt or transform the influence of activity and structure on channel distribution. It is also important to remember that neuronal structure is itself influenced by local Ca^{2+} concentration and activity (23–26). Therefore one ex-

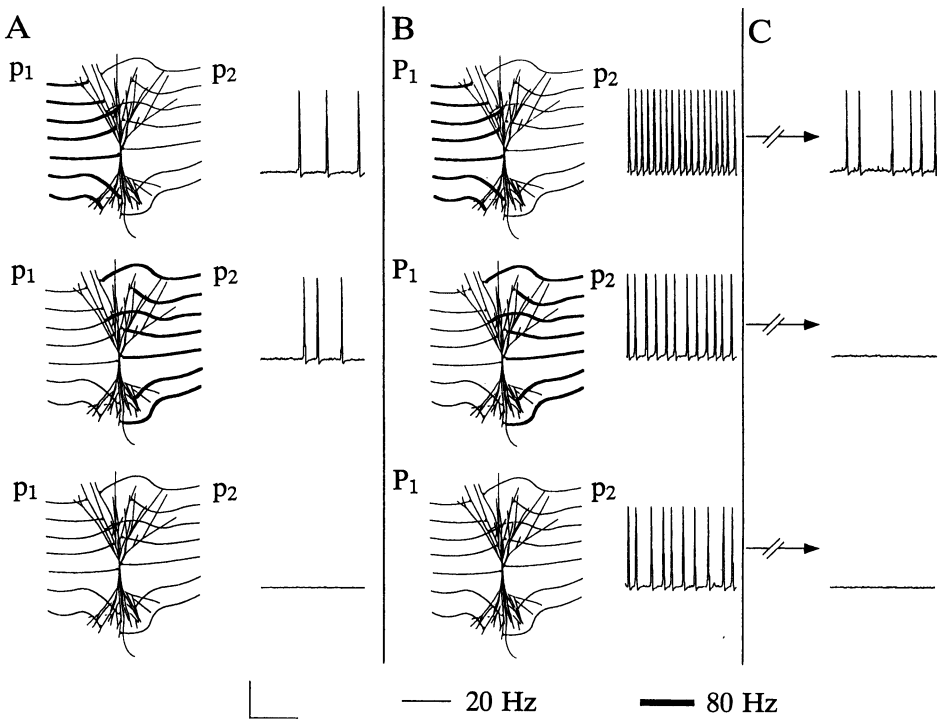

FIG. 3. Regulation of conductances following synaptic potentiation. Synapses were randomly divided into two groups, p_1 and p_2. The three panels in *A*, *B*, and *C* show the response of the model neuron to stimulation of p_1 at 80 Hz and p_2 at 20 Hz (*Top*), p_1 at 20 Hz and p_2 at 80 Hz (*Middle*), and both p_1 and p_2 at 20 Hz (*Bottom*). (*A*) Initial responses before potentiation of p_1 synapses. (*B*) Responses of the same model neuron immediately following potentiation of the p_1 synapses, labeled P_1 to denote potentiation. The increased strength of these synapses caused high-frequency firing (50–90 Hz) for all three stimulation paradigms. (*C*) After a prolonged period of background stimulation (20-Hz stimulation of both P_1 and p_2), represented by the broken arrows, activity-dependent changes in the conductances of the model neuron resulted in the responses shown. The neuron fired when the potentiated P_1 synapses were stimulated at 80 Hz, but not in response to high-frequency stimulation of p_2 or low-frequency stimulation of both patterns. For this figure, we added an I_A (27) to the model to allow for more variation in the firing rate. Activity-dependent regulation of the maximal conductance of I_A was similar to that of I_K. Synaptic conductances were g_{max} = 4 nS for unpotentiated synapses and g_{max} = 8 nS for potentiated synapses. Scale bars: 100 ms and 40 mV.

pects that multiple levels of feedback are called into play to determine how channels are localized in biological neurons.

The model proposed in this paper could, in principle, be tested directly. Because the number and distribution of Na^+-channels can be directly determined with immunoelectron microscopy (22), it should be possible to determine how channel density is affected by local stimulation and correlated with local Ca^{2+} concentration, either in slice or in cultured preparations. Our model predicts that Na^+ channel density should be reduced in regions that show persistent high levels of intracellular Ca^{2+}. There are likely to be neurons in which our simple of model of intracellular Ca^{2+} is highly inaccurate. Nevertheless, in these neurons the prediction that mean Ca^{2+} concentration correlates with channel densities may be valid.

The intrinsic form of activity-dependent plasticity we model here acts more slowly than Hebbian synaptic plasticity, and it has a stabilizing rather than a destabilizing influence on activity. Activity-induced conductance changes may affect regions ranging from around 20 μm to the size of the entire neuron. This reflects the fact that conductances are regulated by both local and global processes. Local effects controlled by local second-messenger concentrations may regulate processes such as vesicle fusion, membrane internalization, and channel phosphorylation to enhance weaker and depress stronger areas of synaptic input, as in Figs. 1*C* and 2. Global modifications involving gene expression and protein synthesis may serve to keep the neuron operating over an appropriate range of firing rates, as in Fig. 3. Acting together, intrinsic plasticity (both local and global mechanisms) and synaptic plasticity produce a system that can store correlations locally, while still retaining sensitivity to all inputs and maintaining a full dynamic range of firing frequencies.

We thank Russ Fricke for providing morphological data for the CA1 pyramidal cell, Zachary F. Mainen for help with our graphical interface, and Michael Hines for writing and generously supporting the public-domain program NEURON. This research was supported by National Institute of Mental Health Grant MH46742 and National Science Foundation Grant DMS-9208206.

1. Kaczmarek, L. K. & Levitan, I. B., eds. (1987) *Neuromodulation: The Biochemical Control of Neuronal Excitability* (Oxford Univ. Press, New York).
2. Kaczmarek, L. K. (1987) *Trends Neurosci.* **10**, 30–34.
3. Alberts, B., Bray, D., Lewis, J., Raff, M., Roberts, K. & Watson, J. D. (1989) *Molecular Biology of the Cell* (Garland, New York).
4. Joe, E. & Angelides, K. (1992) *Nature (London)* **356**, 333–335.
5. Reist, N. E., Werle, M. J. & McMahan, U. J. (1992) *Neuron* **8**, 865–868.
6. Martinou, J., Falls, D. L., Fischbach, G. D. & Merlie, J. P. (1991) *Proc. Natl. Acad. Sci. USA* **88**, 7669–7673.
7. Morgan, J. I. & Curran, T. (1991) *Annu. Rev. Neurosci.* **14**, 421–451.
8. Armstrong, R. C. & Montminy, M. R. (1993) *Annu. Rev. Neurosci.* **16**, 17–30.
9. Murphy, T. H., Worley, P. F. & Baraban, J. M. (1991) *Neuron* **7**, 625–635.
10. Franklin, J. L., Fickbohm, D. J. & Willard, A. L. (1992) *J. Neurosci.* **12**, 1726–1735.
11. Turrigiano, G., Abbott, L. F. & Marder, E. (1994) *Science* **264**, 974–977.
12. LeMasson, G. Marder, E. & Abbott, L. F. (1993) *Science* **259**, 1915–1917.
13. Abbott, L. F. & LeMasson (1993) *Neural Comp.* **5**, 823–842.

14. Hines, M. (1993) in *Neural Systems: Analysis and Modeling*, ed. Eeckman, F. (Kluwer, Norwell, MA), pp. 127–136.
15. Ross, W. M. (1989) *Annu. Rev. Physiol.* **51,** 491–506.
16. Hodgkin, A. L. & Huxley, A. F. J. (1952) *J. Physiol. (London)* **117,** 500–544.
17. Morris, C. & Lecar, H. (1981) *Biophys. J.* **35,** 193–213.
18. Jaffe, D. B., Johnston, D., Lasser-Ross, N., Lisman, J. E., Miyakawa, H. & Ross, W. N. (1992) *Nature (London)* **357,** 244–246.
19. Jaffe, D. B., Ross, W. N. & Johnston, D. (1991) *Soc. Neurosci. Abstr.* **17,** 581.
20. Bell, A. (1992) in *Neural Information Processing Systems 4*, eds. Moody, J. E. & Hanson, S. J. (Morgan Kaufman, San Mateo, CA), pp. 59–66.
21. Regehr, W. G. & Tank, D. W. (1992) *J. Neurosci.* **12,** 4202–4223.
22. Devor, M., Govrin-Lippmann, R. & Angelides, K. (1993) *J. Neurosci.* **13,** 1976–1992.
23. Rehder, V. & Kater, S. B. (1992) *J. Neurosci.* **12,** 3175–3186.
24. Schilling, K., Dickinson, M. H., Connor, J. A. & Morgan, J. I. (1991) *Neuron* **7,** 891–902.
25. Kater, S. B., Mattson, M. P., Cohan, C. & Connor, J. (1988) *Trends Neurosci.* **11,** 315–321.
26. Cohan, C. & Kater, S. B. (1986) *Science* **232,** 1638–1640.
27. Connor, J. A., Walter, D. & Stevens, C. F. (1977) *Biophys. J.* **18,** 81–102.